About "Axial" and "Radial" Diffusivities

Claudia A.M. Wheeler-Kingshott[1]* and Mara Cercignani[1,2]

This article presents the potential problems arising from the use of "axial" and "radial" diffusivities, derived from the eigenvalues of the diffusion tensor, and their interpretation in terms of the underlying biophysical properties, such as myelin and axonal density. Simulated and in vivo data are shown. The simulations demonstrate that a change in "radial" diffusivity can cause a fictitious change in "axial" diffusivity and vice versa in voxels characterized by crossing fibers. The in vivo data compare the direction of the principle eigenvector in four different subjects, two healthy and two affected by multiple sclerosis, and show that the angle, α, between the principal eigenvectors of corresponding voxels of registered datasets is greater than 45° in areas of low anisotropy, severe pathology, and partial volume. Also, there are areas of white matter pathology where the "radial" diffusivity is 10% greater than that of the corresponding normal tissue and where the direction of the principal eigenvector is altered by more than 45° compared to the healthy case. This should strongly discourage researchers from interpreting changes of the "axial" and "radial" diffusivities on the basis of the underlying tissue structure, unless accompanied by a thorough investigation of their mathematical and geometrical properties in each dataset studied. Magn Reson Med 61: 1255–1260, 2009. © 2009 Wiley-Liss, Inc.

Key words: diffusion; axial diffusivity; DTI, eigenvalues;

Since the early publications by Basser et al. (1,2), diffusion tensor imaging (DTI) has evolved and expanded noticeably its application to clinical studies moving toward modeling the tissue microstructure (3–5) and reconstructing white matter tracts (6–8).

While the elements of the tensor matrix are different for each system of coordinates, the DT can be diagonalized to extract its three eigenvalues, λ_1, λ_2, and λ_3, which can be combined to define quantitative parameters such as mean diffusivity (MD) and fractional anisotropy (FA), which are rotationally invariant and independent of eigenvalue sorting.

Since Song et al. (9) published their article where they look at the "axial diffusivity," i.e., the principal eigenvalue of the DT, and at the "radial diffusivity," i.e., the average of the second and third eigenvalues of the DT, in an animal model, and where they link the radial diffusivity with myelin content, studies reporting comparisons of these indices are becoming very frequent (e.g., 10–14). It is important to underline the fact that the direction of the principal eigenvector with eigenvalue λ_1, i.e., the direction of the "axial" diffusivity, is not always preserved in pathological tissue and is not always aligned with the underlying expected tissue architecture (15).

It has been thoroughly shown (e.g., 28) that the direction and the magnitude of the eigenvalues and eigenvectors are physical measures that are affected by the noise, the shape of the calculated diffusion ellipsoid, and pathology. With this study we do not claim to propose a new method for interpreting DTI data or for solving the problem of the sorting bias already extensively investigated (16–18). Here we would like to present a different problem: even if the DT was unaffected by biases, it would be misleading to statistically compare its eigenvalues without checking the alignment of the corresponding eigenvectors with the underlying tissue structures, especially when comparing patients with healthy controls. In other words, if this check is not performed, comparison of the eigenvalues between different subjects or different regions of the same subject (e.g., if one compares the eigenvalues of the contralateral side of a tract affected by pathology) may be meaningless because they could represent completely different physical information. For this reason, we would like to suggest being extremely careful when using the "axial" and "radial" diffusivity terminology as opposed to referring to the eigenvalues of the DT. In fact, given the recognized limitations of the tensor model, we would like to discourage the association between "radial" diffusivity and demyelination, especially in regions of complex tissue architecture.

In order to support our pledge, we use a synthetic model of crossing fibers where we show that pathological changes to the microstructure can result in unpredictable changes to the measured "axial" and "radial" diffusivity, unrelated to the underlying original tissue organization.

Next, we present a simple mathematical test to perform on in vivo data using corresponding voxels of different datasets to highlight areas where the direction of the principal eigenvector $\mathbf{V}_1$ lies in different planes, jeopardizing a direct comparison between the "axial" and "radial" diffusivities.

MATERIALS AND METHODS

Numerical Simulations

1. We modeled two fiber populations crossing at 90° as the superposition of two diffusion tensors with on-diagonal elements $(15, 3, 3) \times 10^{-10} \text{m}^2\text{s}^{-1}$ and $(3, 15, 3) \times 10^{-10}\text{m}^2\text{s}^{-1}$, and zero off-diagonal elements, thus having principal directions parallel to the x and y axes, respectively.

2. Assuming parameters typical of our in vivo data, i.e., a signal-to-noise ratio (SNR) of 16 and a maximum b factor of 1200 s mm^{-2}, for each one of the 61 distributed diffusion directions that we normally acquire, we used Camino (http://www.camino.org.uk) to synthesize 100 voxels from the same two tensors where the initial signal differences between voxels were only due to the added Rician noise. We refer to this dataset as the "baseline" dataset.

[1]UCL Institute of Neurology, Department of Neuroinflammation, London, UK.
[2]Neuroimaging Laboratory, Fondazione Santa Lucia, Rome, Italy.
*Correspondence to: Dr. Claudia A.M. Wheeler-Kingshott, Department of Neuroinflammation, Institute of Neurology, University College London, Queen Square, London WC1N 3BG, UK. E-mail: c.wheeler-kingshott@ion.ucl.ac.uk

3. For the initial two tensors in step 1 and for each voxel in step 2, a single tensor was then fitted to the baseline dataset, and the following measures were derived: FA, axial diffusivity, radial diffusivity, and principal eigenvector.

4. We then went back to step 1 and did the following two simulations:

a. We altered the elements of the second tensor only by increasing the diffusivities along x and z to obtain on-diagonal elements (5, 15, 5) $\times 10^{-10} m^2 s^{-1}$. This simulates an increase in the "radial" component of the second tensor only, which could result from secondary white matter degeneration (19) of a single fiber bundle. We refer to this dataset as the "demyelinated" dataset.

b. We altered the elements of the second tensor only by decreasing the diffusivity along y to obtain on-diagonal elements (3, 12, 3) $\times 10^{-10} m^2 s^{-1}$. This simulates a decrease in the "axial" component of the second tensor only, aligned with y, which could result from axonal degeneration of a single fiber bundle. We refer to this dataset as the "axonal degeneration" dataset.

We then repeated steps 2 and 3 and compared FA, axial diffusivity, radial diffusivity, and the direction of the principal eigenvector between the two datasets to ascertain the ability of "radial" and "axial" diffusivity to provide specific information about pathology in areas where the underlying microstructure is complex.

In Vivo Data

Acquisition

Two healthy controls (females, ages 35 (HC_{ref}) and 37 (HC) years old, respectively) and two patients with relapsing remitting multiple sclerosis (MS) (a female, age 34 (MS_{p1}) disease duration = 1.5 years, EDSS (Expanded Disability Status Scale) = 2.5, and a male, age 55 (MS_{p2}) disease duration = 7 years, EDSS = 5.5) were scanned on a 1.5T GE Signa MRI scanner (General Electric, Milwaukee, WI) with a maximum gradient strength of 33 mT m^{-1}. An 8-channel phased-array coil was used as receiver, while the whole body coil was used as transmitter.

A cardiac gated diffusion-weighted spin-echo echo planar imaging (DW-SE-EPI) sequence was used to acquire the diffusion weighted data with diffusion weighting applied along 61 directions with b-factor = 1200 s mm^{-2}, interleaved with seven nondiffusion weighted 60 acquisitions, 60 axial slices prescribed parallel to the anterior commissure − posterior commissure (AC-PC) line, field of view (FOV) = 220 mm, matrix = 96 × 96 (reconstructed to 128 × 128), in-plane resolution = 2.3 × 2.3 mm^2 (reconstructed to 1.71 × 1.71mm^2), slice thickness = 2.3 mm, TR = 20 RRs 20 sec (depending on the cardiac cycle rate), TE = 84.8 ms, total acquisition time 20 min. Standard proton density (PD) and T_2-weighted images were also acquired.

Analysis

We generated maps of the angle between the principal eigenvector of the reference dataset and the principal eig-

envector of each one of the other three datasets as follows. One of the two healthy controls (HC_{ref}) was used as the reference for intersubject registration (see step 3 below):

1. Intrasubject registration: eddy currents-induced distortions and small head motions were corrected using 3D affine registration (see eddycorrect, FMRIB Diffusion Toolbox (FDT) http://www.fmrib.ox.ac.uk/fsl/fdt/index.html).

2. Tensor fitting: the DT was fitted to the output of step 1 (using the dtfit routine of FMRIB FDT) and FA was computed for every subject.

3. Intersubject registration: every subject's FA was matched to that of HC_{ref} (FA_{ref}) by affine followed by nonlinear registration (see FLIRT and FNIRT, http://www.fmrib.ox.ac.uk/fsl/fsl/list.html). The transformations were then applied to each component of the DT using the PPD (preservation of principal direction) algorithm (20). The rotated DT was used to generate the eigenvalues and the eigenvectors (in the common space defined by HC_{ref}), $\lambda_1(i)$, $\lambda_2(i)$, $\lambda_3(i)$ and $V_1(i)$, $V_2(i)$, $V_3(i)$, respectively, where "i" represents each one of the four datasets (i = HC_{ref} for the reference healthy control, i = HC for the other healthy control, i = MS_{p1} for the first MS patient, and i = MS_{p2} for the second MS patient).

4. Estimation of angle: for each voxel of the data registered to the reference volume, the cosine of the angle $\alpha(i)$ between $V_1(HC_{ref})$ and the principal eigenvector $V_1(i)$ of each one of the other subjects was calculated as the scalar product of $V_1(HC_{ref})$ and $V_1(i)$, where the index "i" is defined as in step 3.

5. Thresholding α: The maps of α generated in step 4 were then thresholded to highlight voxels where $|\alpha(HC_{ref}, i)| > 45°$, i.e., $|\cos \alpha(HC_{ref}, i)| < 0.7$. The threshold of 45° was arbitrarily chosen to represent a deviation from coherence that is well above the expected cone of uncertainty of highly anisotropic structures, previously reported as low as 3° in the splenium of the corpus callosum and 10° in the frontal white matter areas (18).

6. Thresholding FA: We thresholded all the registered FA maps to create a mask of common voxels with FA >0.3 and we highlighted voxels where the "radial" diffusivity of the MS_{p2} was increased by 10% compared with that of HC_{ref} while the angle between their corresponding principal eigenvectors α was greater than 45°.

RESULTS

Numerical Simulations

The single tensor model yielded an estimated direction of the main eigenvectors randomly ranging between x and y (Fig. 1b,c), depending on the noise, for the "baseline" dataset. For both the "demyelinated" and "axonal degeneration" datasets, the single-tensor fitting returned the principal direction of diffusion to be mainly parallel to x (Fig. 1b',c',b",c"). When comparing scalar indices between the two datasets (see Table 1), in the "demyelinated" case both "axial" and "radial" diffusivities were found to be increased, while FA was found to be reduced compared to
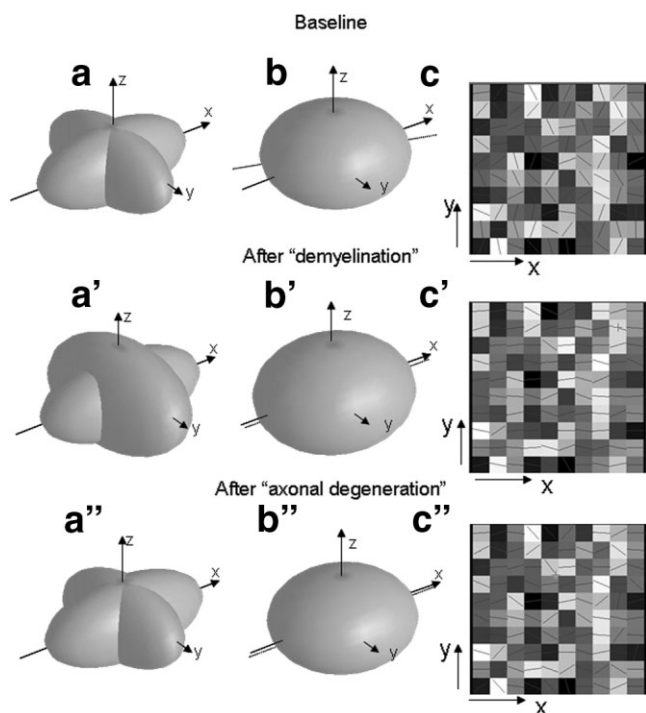
FIG. 1. **a:** The two tensor ellipsoids used to simulate the data (Table 1, original tensors A and B). **b:** Tensor ellipsoid resulting from fitting the data simulated using the tensors in **(a)** with a single tensor in absence of noise. The light-gray line indicates the direction of the principal eigenvector. **c:** Estimated direction of the principal eigenvector, overlaid onto FA, in 100 voxels where we modeled the two tensors in **(a)** and added noise before fitting a single tensor. **a':** Two tensors model where we changed the radial component of the tensor representing the fibers aligned with the y axis. **b':** Fitting of **(a')** with a single tensor in absence of noise. The change in the "radial" diffusivity of the tensor with principal eigenvector aligned with y has changed the overall single tensor shape so that the principle eigenvector of the single tensor now is effectively aligned with the "healthy" fiber (aligned with x). **c':** The same as in **(c)** but for the two tensors defined in **(a')**. **a'':** Two tensors ellipsoids where we changed the axial component of the tensor representing the fibers aligned with the y axis. **b'':** Fitting of **(a'')** with a single tensor in absence of noise. The estimated direction in the absence of noise is coincident with x axis. **c'':** The same as in **(c)** but for these two tensors.

the baseline. Moreover, the mean change in the estimated direction of the principal eigenvalue was 57.3°. In the "axonal degeneration" dataset, we found similarly unexpected results, where both "axial" and "radial" diffusivities of the single tensor were both reduced by the changes in the "axial" component of one of the underlying crossing tensors (Fig. 1b'',c''). In this example, too, the direction of the principal eigenvector was changed on average by 42.9° compared to the initial one.

In Vivo Data

The maps of $\alpha(HC_{ref}, HC)$ (Fig. 2a), corresponding to voxels with FA >0.3, show that there is good agreement between the direction of the principal eigenvector in the major white matter tracts of two healthy controls (i.e., $\alpha(HC_{ref}, HC) < 45°$), with a few sparse voxels in white matter areas

that show misalignment >45°. The comparison of MS_{p1}, with a relatively low lesion load and low EDSS, with HC_{ref} showed that there are areas in white matter (FA >0.3) where there is a clear change in the direction of the principal eigenvector with $|\alpha(HC_{ref}, MS_{p1})| > 45°$ (Fig. 2b). These areas do not coincide necessarily with MS lesions and can be located within the normal appearing white matter (NAWM). The same comparison between MS_{p2} and HC_{ref} shows a greater number of voxels with $\alpha(HC_{ref}, MS_{p2})| > 45°$ even in voxels with FA >0.3 (Fig. 2c).

Figure 2d–f shows a sagittal view of a problematic area with a different distribution of directions between the subjects (HC_{ref} (d), HC (e), and MS_{p1} (f), respectively), where the greatest difference, though, is between HC_{ref} and MS_{p1}.

The comparison of MS_{p2} with HC_{ref} showed several areas of white matter that are characterized by a difference in the direction of the principal eigenvector with $|\alpha(HC_{ref}, MS_{p2})| > 45°$. These areas include both normal-appearing white matter and white matter lesions (Fig. 2i). A close-up look at a color-coded map of the direction of V_1 in the corpus callosum shows very clearly the different orientation that V_1 assumes in MS_{p2} compared to HC_{ref} (Fig. 2g,h).

For each subject, i = HC, MS_{p1}, MS_{p2}, we also tested whether there were voxels with a "radial" diffusivity change >10% compared to radial diffusivity of HC_{ref} accompanied by a change of the direction of the principal eigenvector with $|\alpha(HC_{ref}, i)| > 45°$. Given the potentially problematic anatomical difference, which is only partially compensated by image registration, the figure only displays voxels where FA >0.3. Voxels with these characteristics are plotted on FA_{ref} in Fig. 2j–l, showing that they cover areas where partial volume, misregistration, and anatomical differences could be counted responsible for them. Nevertheless, from Fig. 2i,k,l it appears that MS_{p2} has more extensive regions of white matter where the "radial" diffusivity has increased and the direction of the principal eigenvector has changed compared to MS_{p1} and HC.

DISCUSSION

This study confirms that the eigenvalues of the DT, λ_1, λ_2, and λ_3, do not necessarily reflect the same underlying structural characteristics in different datasets because of a different orientation of the corresponding principal eigenvector, V_1. This happens especially in areas of low anisotropy such as gray matter, voxels affected by partial volume, areas of crossing fibers, or where the diffusion ellipsoid is oblate, i.e., where V_1 is characterized by a large cone of uncertainty. Similar results have been shown by others in other pathologies [15], supporting the inadequacy of scalar quantities such as "radial" diffusivity based on λ_2 and λ_3 to characterize myelin content, unless accompanied by a thorough investigation of the principal direction of diffusion.

Whether the measured direction of V_1 differs between subjects because of pathology, crossing fibers, or residual misalignment that even nonlinear registration cannot completely eliminate, the point is that in such voxels comparing the absolute value of λ_1 and consequently of the average of λ_2 and λ_3 can be meaningless because the same

Table 1
Results of the Simulations

	90° crossing, 50% contribution	90° crossing, 50% contribution
Original tensor A	$0.5 \begin{bmatrix} 3 & 0 & 0 \\ 0 & 15 & 0 \\ 0 & 0 & 3 \end{bmatrix}$	$0.5 \begin{bmatrix} 15 & 0 & 0 \\ 0 & 3 & 0 \\ 0 & 0 & 3 \end{bmatrix}$
Original tensor B	$0.5 \begin{bmatrix} 15 & 0 & 0 \\ 0 & 3 & 0 \\ 0 & 0 & 3 \end{bmatrix}$	$0.5 \begin{bmatrix} 3 & 0 & 0 \\ 0 & 15 & 0 \\ 0 & 0 & 3 \end{bmatrix}$
Alteration	Increase "radial" components of tensor B	Reduce "axial" component of tensor B
Resulting tensor A	$0.5 \begin{bmatrix} 15 & 0 & 0 \\ 0 & 3 & 0 \\ 0 & 0 & 3 \end{bmatrix}$	$0.5 \begin{bmatrix} 15 & 0 & 0 \\ 0 & 3 & 0 \\ 0 & 0 & 3 \end{bmatrix}$
Resulting tensor B	$0.5 \begin{bmatrix} 5 & 0 & 0 \\ 0 & 15 & 0 \\ 0 & 0 & 5 \end{bmatrix}$	$0.5 \begin{bmatrix} 3 & 0 & 0 \\ 0 & 12 & 0 \\ 0 & 0 & 3 \end{bmatrix}$
Effect on indices estimated by fitting a single tensor		
Mean* percentage change in "radial" diffusivity	↑ (+9.3±2.9%)	↓ (−6.6±1.83%)
Mean* percentage change in "axial" diffusivity	↑ (+13.7±4%)	↓ (−5.32±2.43%)
Mean* percentage change in FA	↓ (−9.6±3.3%)	↓ (−3.4±1.63%)
Mean* change in the direction of principal eigenvector, V_1	57.3°	42.9°

The mean values (*) are calculated over the simulated 100 voxels.

physical quantity may represent different biophysical substrates in different DT datasets. This may be due to a real change of the main structure or it may be the result of a sorting bias or simply the effect of structural differences between subjects not eliminated by the registration step. Although the synthetic model of crossing fibers we used is simplistic, it shows how dangerous it can be to assume a direct correspondence between changes to the eigenvalues, which are properties of the tensor, and a pathological substrate such as demyelination and/or axonal loss, in areas where the tensor does not describe tissue microstructure adequately. Changes in diffusivities along and across fiber bundles do indeed occur, but the interpretation of such changes is not obvious, and the direction of the change may vary according to the specific microscopic geometry.

Considering the cone of uncertainty in the measure of V_1, one could argue that if the uncertainty is generated by a real geometry of the underlying tissue structure, then any direction of V_1 within the cone would have the same eigenvalue. In light of this, one could justify the comparison of λ_1 between datasets as long as the angle between the principle eigenvectors was within the cone of uncertainty.

We believe, though, that even in an ideal case where one could measure the eigenvectors and eigenvalues of the DT with extremely high precision, pathology could change the direction of the principal eigenvector with respect to the underlying structures. This scenario is clearly demonstrated in Fig. 1b,b',b''. After modeling "demyelination" of one of the tracts, by changing the radial diffusivity of one of the two initial tensors, the estimated direction of V_1 is

altered by more than 50%, with a 9% increase of the radial diffusivity and 20% increase of axial diffusivity of the fitted single tensor. A similar result is obtained when simulating a change in the axial diffusivity of one of the two crossing tensors, as shown in Table 1. Hence, the interpretation of the changes of the eigenvalues as "demyelination" or "axonal degeneration" is inappropriate because in pathological tissue V_1 may change alignment, hence representing a different substrate. An example of a similar situation is reported by Schwartzman et al. (21), who showed a significant difference in the direction of the principal eigenvector in a group of poor readers compared to good readers. Whatever the reason for the misalignment of V_1, this problem underpins the rationale behind the definition of "axial" and "radial" diffusivities and their interpretation in relation to histology results of myelin content and axonal density measures.

Errors could be avoided by considering maps of α as indicative of areas to exclude when comparing the principal eigenvalues of the diagonalized DT, because of possible directionality changes in well-defined white matter tracts or to highlight areas of low anisotropy due to a complicated underlying structure, such as crossing fibers, where comparisons of λ_1 between datasets may be misleading.

Other authors have proposed different approaches, such as developing statistical tools that permit the direct comparison of the main direction of diffusion, as well as of the eigenvalues (e.g., 21,22). Unfortunately, these methods are complex and not generally available to clinical researchers.

As a general observation, we wish to stress that, although it is tempting to speculate about the underlying
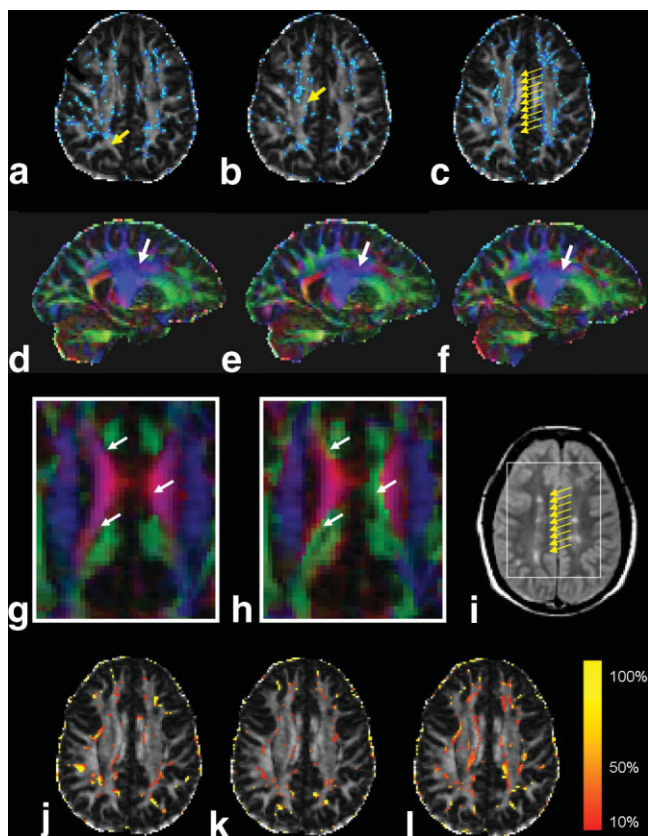
FIG. 2. **a–c:** The blue voxels are those where $\alpha > 45°$ and FA > 0.3, with α representing the angle between $\mathbf{V}_1(HC_{ref})$ and $\mathbf{V}_1(HC)$ in **a)**, between $\mathbf{V}_1(HC_{ref})$ and $\mathbf{V}_1(MS_{p1})$ in **b)**, and between $\mathbf{V}_1(HC_{ref})$ and $\mathbf{V}_1(MS_{p2})$ in **c)** overlaid on the axial FA map of HC_{ref}. The arrows indicate examples of white matter area where $\alpha > 45°$ between the principal eigenvector of an HC, MS_{p1} and MS_{p2} with HC_{ref}. **d–f:** Sagittal FA maps of HC_{ref} overlaid with the $\mathbf{V}_1$ color map of HC_{ref}, HC, and MS_{p1} at the same position in the registered brains. The colors represent the direction of $\mathbf{V}_1$ (red: right/left, green: anterior/posterior, blue: superior/inferior). The images show how different the direction of $\mathbf{V}_1$ is in corresponding voxels between subjects, with the pathological brain being the most different. In particular, the arrow indicates an example of area where there is an anatomical difference in the principal eigenvector's orientation between HC_{ref}, HC, and MS_{p1}. **g,h:** A close-up of the area represented by the white square on the PD-weighted image **(i)**, showing the direction of $\mathbf{V}_1$ in HC_{ref} (image **g**) and in MS_{p2} (image **h**). The color-coding is the same as in **(d–f)**. The arrows indicate a few examples of almost orthogonal $\mathbf{V}_1$ between the patient MS_{p2} and the control HC_{ref}. **j–l:** Axial FA_{ref} maps overlaid with voxels characterized by an increase of the "radial" diffusivity value $>10\%$ compared to that of HC_{ref} and $|\alpha(HC_{ref}, i)| > 45°$, where i = HC (Fig. **j**), MS_{p1} (Fig. **k**), MS_{p2} (Fig. **l**) for voxels where FA >0.3. The color bar indicates the percent variation of radial diffusivity compared to HC_{ref}.

pathological substrate of changes in DTI-derived parameters, it is extremely difficult to univocally associate them with specific biophysical changes without a spatially matching postmortem examination of each case. Furthermore, interpretations and theories behind changes of indices that are sensitive to the sorting of the eigenvectors or to the effect of noise and partial volume, such as the "axial" and "radial" diffusivities, should be discouraged unless

accompanied by a thorough investigation of their mathematical and geometrical properties.

REFERENCES

1. Basser PJ, Mattiello J, LeBihan D. MR diffusion tensor spectroscopy and imaging. Biophys J 1994;66:259–267.
2. Mattiello J, Basser PJ, Le Bihan D. Analytical expressions for the b matrix in NMR diffusion imaging and spectroscopy. J Magn Reson A 1994;131–141.
3. King MD, Houseman J, Roussel SA, Vanbruggen N, Williams SR, Gadian DG. Q-space imaging of the brain. Magn Reson Med 1994;32:707–713.
4. Basser PJ. Relationships between diffusion tensor and q-space MRI. Magn Reson Med 2002;47:392–397.
5. Tuch DS. Q-ball imaging. Magn Reson Med 2004;52:1358–1372.
6. Mori S, Crain BJ, Chacko VP, van Zijl PC. Three-dimensional tracking of axonal projections in the brain by magnetic resonance imaging. Ann Neurol 1999;45:265–269.
7. Conturo TE, Lori NF, Cull TS, Akbudak E, Snyder AZ, Shimony JS, McKinstry RC, Burton H, Raichle ME. Tracking neuronal fiber pathways in the living human brain. Proc Natl Acad Sci U S A 1999;96:10422–10427.
8. Parker GJ, Stephan KE, Barker GJ, Rowe JB, MacManus DG, Wheeler-Kingshott CA, Ciccarelli O, Passingham RE, Spinks RL, Lemon RN, Turner R. Initial demonstration of in vivo tracing of axonal projections in the macaque brain and comparison with the human brain using diffusion tensor imaging and fast marching tractography. Neuroimage 2002;15:797–809.
9. Song SK, Sun SW, Ramsbottom MJ, Chang C, Russell J, Cross AH. Dysmyelination revealed through MRI as increased radial (but unchanged axial) diffusion of water. Neuroimage 2002;17:1429–1436.
10. Ashtari M, Cervellione KL, Hasan KM, Wu J, McIlree C, Kester H, Ardekani BA, Roofeh D, Szeszko PR, Kumra S. White matter development during late adolescence in healthy males: a cross-sectional diffusion tensor imaging study. Neuroimage 2007;35:501–510.
11. Choi SJ, Lim KO, Monteiro I, Reisberg B. Diffusion tensor imaging of frontal white matter microstructure in early Alzheimer's disease: a preliminary study. J Geriatr Psychiatry Neurol 2005;18:12–19.
12. Counsell SJ, Shen Y, Boardman JP, Larkman DJ, Kapellou O, Ward P, Allsop JM, Cowan FM, Hajnal JV, Edwards AD, Rutherford MA. Axial and radial diffusivity in preterm infants who have diffuse white matter changes on magnetic resonance imaging at term-equivalent age. Pediatrics 2006;117:376–386.
13. Deboy CA, Zhang J, Dike S, Shats I, Jones M, Reich DS, Mori S, Nguyen T, Rothstein B, Miller RH, Griffin JT, Kerr DA, Calabresi PA. High resolution diffusion tensor imaging of axonal damage in focal inflammatory and demyelinating lesions in rat spinal cord. Brain 2007;130:2199–2210.
14. Schmierer K, Wheeler-Kingshott CA, Boulby PA, Scaravilli F, Altmann DR, Barker GJ, Tofts PS, Miller DH. Diffusion tensor imaging of post mortem multiple sclerosis brain. Neuroimage 2007;35:467–477.
15. Field AS, Alexander AL, Wu YC, Hasan KM, Witwer B, Badie B. Diffusion tensor eigenvector directional color imaging patterns in the evaluation of cerebral white matter tracts altered by tumor. J Magn Reson Imaging 2004;20:555–562.

16. Basser PJ, Pajevic S. Statistical artifacts in diffusion tensor MRI (DT-MRI) caused by background noise. Magn Reson Med 2000;44: 41–50.

17. Martin KM, Papadakis NG, Huang CL, Hall LD, Carpenter TA. The reduction of the sorting bias in the eigenvalues of the diffusion tensor. Magn Reson Imaging 1999;17:893–901.

18. Jones DK. Determining and visualizing uncertainty in estimates of fiber orientation from diffusion tensor MRI. Magn Reson Med 2003;49:7–12.

19. Pierpaoli C, Barnett A, Pajevic S, Chen R, Penix LR, Virta A, Basser P. Water diffusion changes in Wallerian degeneration and their dependence on white matter architecture. Neuroimage 2001;13: 1174–1185.

20. Alexander DC, Pierpaoli C, Basser PJ, Gee JC. Spatial transformations of diffusion tensor magnetic resonance images. IEEE Trans Med Imaging 2001;20:1131–1139.

21. Schwartzman A, Dougherty RF, Taylor JE. Cross-subject comparison of principal diffusion direction maps. Magn Reson Med 2005;53:1423–1431.

22. Pajevic S, Basser PJ. Parametric and non-parametric statistical analysis of DT-MRI data. J Magn Reson 2003;161:1–14.